X-ray absorption spectra: Graphene, *h*-BN, and their alloy

Somnath Bhowmick,* Jan Rusz,† and Olle Eriksson‡
Department of Physics and Astronomy, Uppsala University, P.O. Box 516, 75120 Uppsala, Sweden
(Received 2 December 2012; revised manuscript received 13 February 2013; published 3 April 2013)

Using first-principles density functional theory calculations, in conjunction with the Mahan–Nozières–de Dominicis theory, we calculate the x-ray absorption spectra of the alloys of graphene and monolayer hexagonal boron nitride on a Ni (111) substrate. The chemical neighborhood of the constituent atoms (B, C, and N) inside the alloy differs from that of the parent phases. In a systematic way, we capture the change in the *K*-edge spectral shape, depending on the chemical neighborhood of B, C, and N. Our work also reiterates the importance of the dynamical core-hole screening for a proper description of the x-ray absorption process in sp^2-bonded layered materials.

DOI: 10.1103/PhysRevB.87.155108 PACS number(s): 73.61.Wp, 68.65.Cd, 78.70.Dm, 79.60.Jv

Graphene was the first truly two-dimensional material discovered and it enjoyed a tremendous amount of attention, in terms of both the fundamental physics and device applications.[1–4] It was soon followed by others, such as its isoelectronic sibling, monolayer hexagonal boron nitride (*h*-BN; hexagonal in the sense of a two-dimensional Bravais lattice).[4–7] One of the most popular methods for the growth of such materials is chemical vapor deposition on various metal substrates, such as the (111) surface of Ni and Cu.[8–11] The metal substrate is often etched after the growth process and the monolayer is transferred to some other insulating substrate.[12] The honeycomb lattice is formed by placing an atom (C, B, or N) and its nearest neighbor on top of the nickel and fcc hollow site, respectively. The lattice parameter of nickel is such that the mismatch is less than $\pm 1\%$ between the honeycomb lattice formed by graphene or *h*-BN on a Ni substrate and their free-standing counterparts.[13] This ensures minimal distortions, such as warping and moiré patterns, observed in the case of a lattice-mismatched substrate such as copper.[11]

In terms of their electronic properties, graphene and monolayer *h*-BN are at two opposite extremes. While graphene is semimetallic and a very good conductor, *h*-BN is a very good insulator. In the recent past, there have been several attempts to fabricate alloys of graphene and *h*-BN.[12] Such materials maintain the honeycomb lattice structure and their electronic properties lie in between those of the parent phases, which provides much needed tunability for device applications.[12] Depending on the process parameters, a material of a given composition $B_xC_yN_z$ can either form an alloy or phase separate.[12,14,15] Among the alloys, BC_2N has been studied most extensively.[14–20]

X-ray absorption spectroscopy (XAS) is an experimental technique widely used to characterize the electronic structure of sp^2-bonded layered materials like graphene and monolayer *h*-BN and the spectra have been successfully calculated using *ab initio* electronic structure calculations.[21,22] The ability to reliably interpret XAS spectra of a newly prepared $B_xC_yN_z$ monolayer on a Ni(111) substrate will allow the nature of the material—alloy vs phase separated—to be judged prior to its transfer to other substrates.

During the x-ray absorption process, the system undergoes a transition from the initial ground state (without core hole) to the final excited state (with core hole). Some qualitative features of the spectra can be interpreted in terms of the electronic density of states (DOS) of the initial and final states. However, such a simple approach excludes many complicated many-body processes involved in XAS.[23] Instead of approximating the photon-electron interaction as a diabatic (initial-state DOS) or adiabatic (final-state DOS) process, a more realistic theory was proposed by Mahan–Nozières–de Dominicis (MND) that takes into account the actual dynamics of the core-hole screening.[23,24] In this regard, it is worth mentioning the work of Privalov *et al.*,[25,26] who showed a practical way of using the MND theory by reducing the MND equations to a set of linear algebraic equations. Compared to the methods based on the initial, final, or Slater transition state,[27] MND theory provided better description of the XA spectra at computational costs much lower than other state-of-the-art methods, such as the Bethe-Salpeter equation or time-dependent density functional theory (DFT) calculations. Recently, the MND theory was implemented on top of first-principles density functional theory calculations[28,29] and applied to monolayer graphene or hexagonal boron nitride on a Ni(111) substrate.[30] We have employed a similar method to calculate the XA spectra, based on the MND theory formulated in the energy representation.[31]

Given an arbitrary stoichiometry of $B_xC_yN_z$, there are innumerable choices of unit cells. Exhausting all of them is beyond the scope of any theoretical investigation. As mentioned previously, BC_2N is the material studied most intensely and our investigation is focused on it. As the smallest structural model of an alloy, it represents the antipole of a completely phase-separated compound consisting of large grains of pure *h*-BN and graphene. The chosen atomic arrangements are shown in Figs. 1(a) (named BC_2N^I) and 1(b) (named BC_2N^{II}). For a free-standing monolayer of BC_2N, these are the two most energetically favorable structures.[16] For better understanding, we also report the spectra for graphene, monolayer *h*-BN, and two "fictitious" materials, monolayer hexagonal BC and NC.[32] Our line of investigation helps to reveal, in a systematic way, the change of XAS shape of an atom, depending on its neighbors. For example, a C atom has three C neighbors (graphene); two C neighbors and one B/N neighbor (in BC_2N^I); one C and two B/N neighbors (in BC_2N^{II}); three B/N neighbors (in BC/NC). Moreover, the underlying substrate adds two additional degrees of

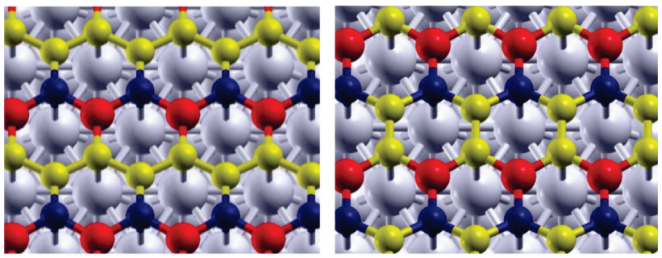

(a)BC_2N^I (b)BC_2N^{II}

FIG. 1. (Color online) Atomic arrangements of monolayer BC_2N on top of a Ni substrate (gray in color). B, C, and N atoms are shown in red, yellow, and blue, respectively. As per our calculations (see text for details), the configurations with N on top of the Ni atom and B on top of the fcc hollow site are lower in energy and they are shown in the above diagram. The other possible set, i.e., B on top of the Ni atom and N on top of the fcc hollow site (not illustrated here), are denoted by BC_2N^{IH} and BC_2N^{IIH}.

freedom in terms of possible atomic arrangements, because any constituent atom can be placed on top of either the Ni or fcc hollow site (see the caption of Fig. 1). In this work, we exhaust all such possibilities, and thus report a comprehensive theoretical study of the XAS spectrum of a B-C-N (arranged in a honeycomb lattice) monolayer, deposited on a Ni(111) substrate.

The substrate is represented by three layers of nickel atoms. We have verified that the substrate thickness is large enough to capture the substrate-monolayer interaction accurately. For example, the substrate-monolayer distance is nearly the same, irrespective of the number of nickel layers (three to six). To simulate the properties of monolayer of a BC_2N on a Ni(111) surface, we keep ∼15 Å of vacuum layer between the two copies of periodic images in the direction perpendicular to the plane of the substrate. All the geometry optimizations are performed using the QUANTUM ESPRESSO code,[33] using a plane-wave basis set and ultrasoft pseudopotential. Electron exchange and correlation were treated within the framework of the Perdew-Burke-Ernzerhof generalized gradient approximation. We set the kinetic energy cutoff for the wave functions to be 40 Ry. The Brillouin zone was sampled using $28 \times 16 \times 1$ k points. We relax the structures fully until the force on

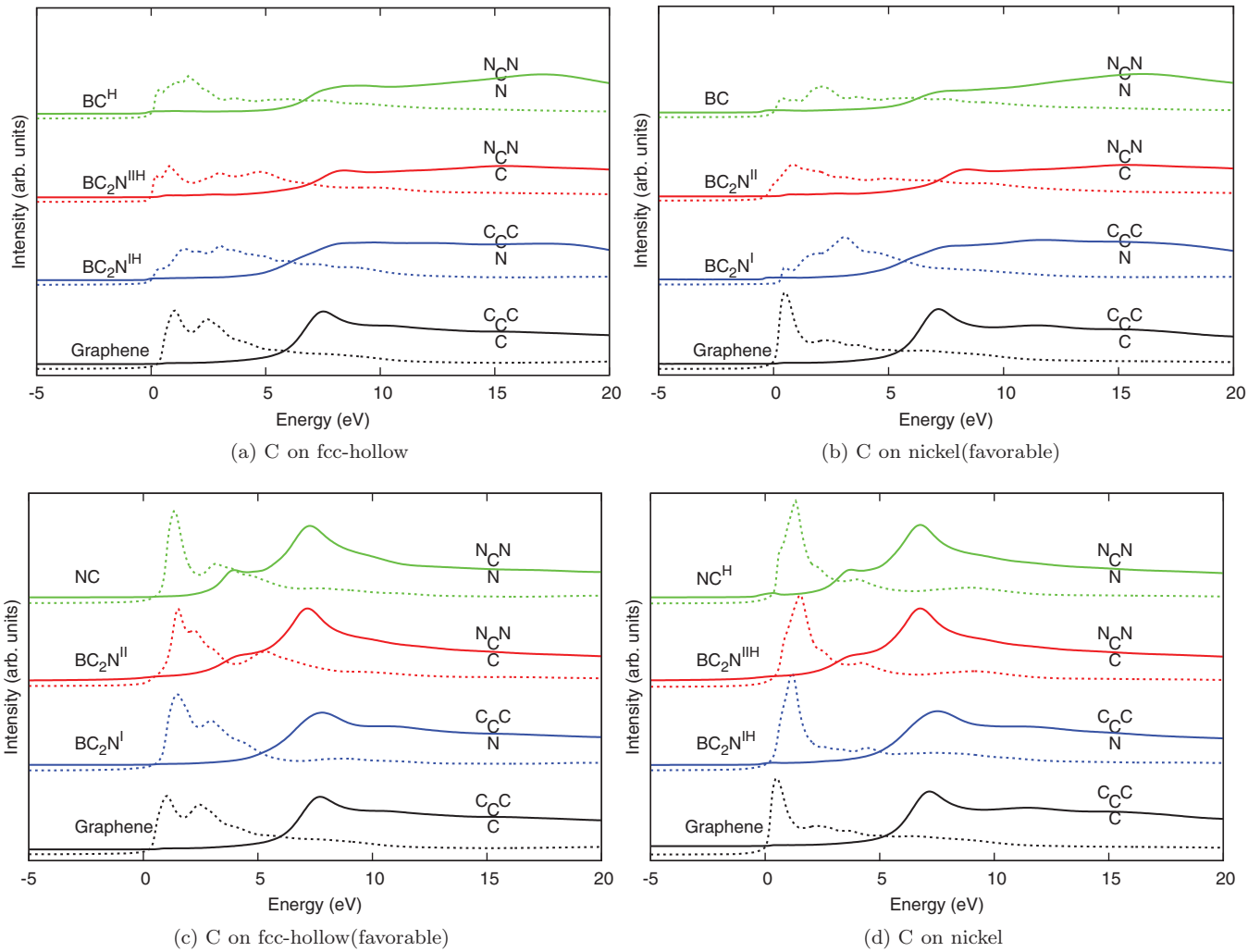

(a) C on fcc-hollow (b) C on nickel(favorable)

(c) C on fcc-hollow(favorable) (d) C on nickel

FIG. 2. (Color online) 1s x-ray absorption spectra of a carbon atom; in graphene, two types of BC_2N unit cells shown in Fig. 1, and BC/NC. The chemical environment of the excited atom (with a core hole) is shown schematically, with the atom located at the center and its three nearest neighbors. The solid (dotted) line represents the $\sigma^\star$ ($\pi^\star$) contribution to the XAS spectra.

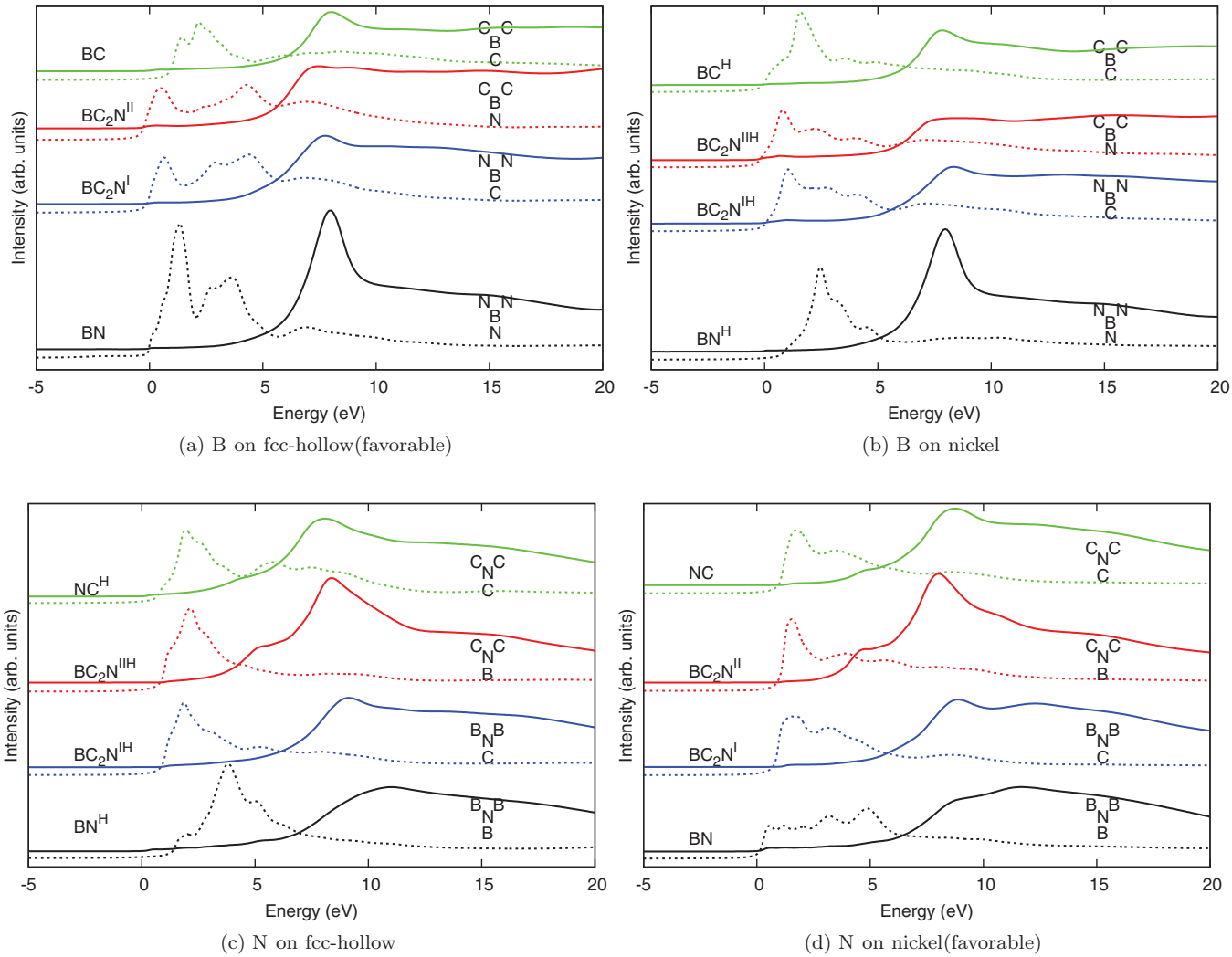

(a) B on fcc-hollow(favorable) (b) B on nickel

(c) N on fcc-hollow (d) N on nickel(favorable)

FIG. 3. (Color online) 1*s* x-ray absorption spectra of (a), (b) boron and (c), (d) nitrogen atoms; in *h*-BN, two types of BC_2N unit cells shown in Fig. 1, and BC/NC.

each atom (the total energy change for ionic minimization) is less than 10^{-3} Ry/a.u. (10^{-4} Ry). We have verified that the charge transfers between the Ni and the BC_2N monolayer are negligible; hence no significant dipole barrier was established. This allowed us to work with smaller structural models compared to "sandwich" structures with BC_2N monolayers on both sides of the substrate slab.

Our structural relaxation results are consistent with previous works, as reported in the literature. For example, we correctly find that N on top of Ni and B on top of the fcc hollow position is energetically more favorable than the reverse, in the case of monolayer *h*-BN deposited on a Ni substrate.[27] Our study reveals a similar scenario also in the case of a BC_2N monolayer on a Ni substrate. The lowest energy structures are shown in Figs. 1(a) and 1(b), both having N on top of Ni and B on the fcc hollow site. These structures are ∼20 meV/atom lower in energy than that of B on top of the Ni and N on top of the fcc hollow unit cells (denoted by BC_2N^{IH}, BC_2N^{IIH}, BN^H, BC^H, and NC^H in the text, where the superscript H stands for higher energy). Moreover, between the two unit cells shown in Fig. 1, BC_2N^I is energetically more favorable than BC_2N^{II} (by ∼4 meV/atom). Note that this energy difference is rather small and thus its exact value may be sensitive to numerical details of the electronic structure calculations. Therefore we have calculated XA spectra for both structure models.

As inputs to the MND model, we need to provide local Green's function matrices $\langle a;l'm's'|G(E)|a;lms\rangle = \sum_{\mathbf{k}n}\langle a;l'm's'|\mathbf{k}n\rangle(E-E_{\mathbf{k}n}+i\mu)^{-1}\langle\mathbf{k}n|a;lms\rangle$ of the electronic structure for the initial (no core hole) and final (in the presence of a core hole) states. Here, a denotes the atom for which the local electronic structure is evaluated, $E_{\mathbf{k}n}$ is the energy of a Bloch state with wave vector $\mathbf{k}$ and band index n, and l, m, and s are the angular, magnetic, and spin quantum numbers in the local coordinate frame of the atom a. We have performed all the electronic structure and spectral calculations using the WIEN2K code,[34] where the relaxed structures from the previous set of quantum ESPRESSO calculations were used. WIEN2K is an all-electron full-potential electronic structure code. It makes no approximations about the shape of potential or density and includes full relaxation of the core states throughout the self-consistent cycle. It also allows true

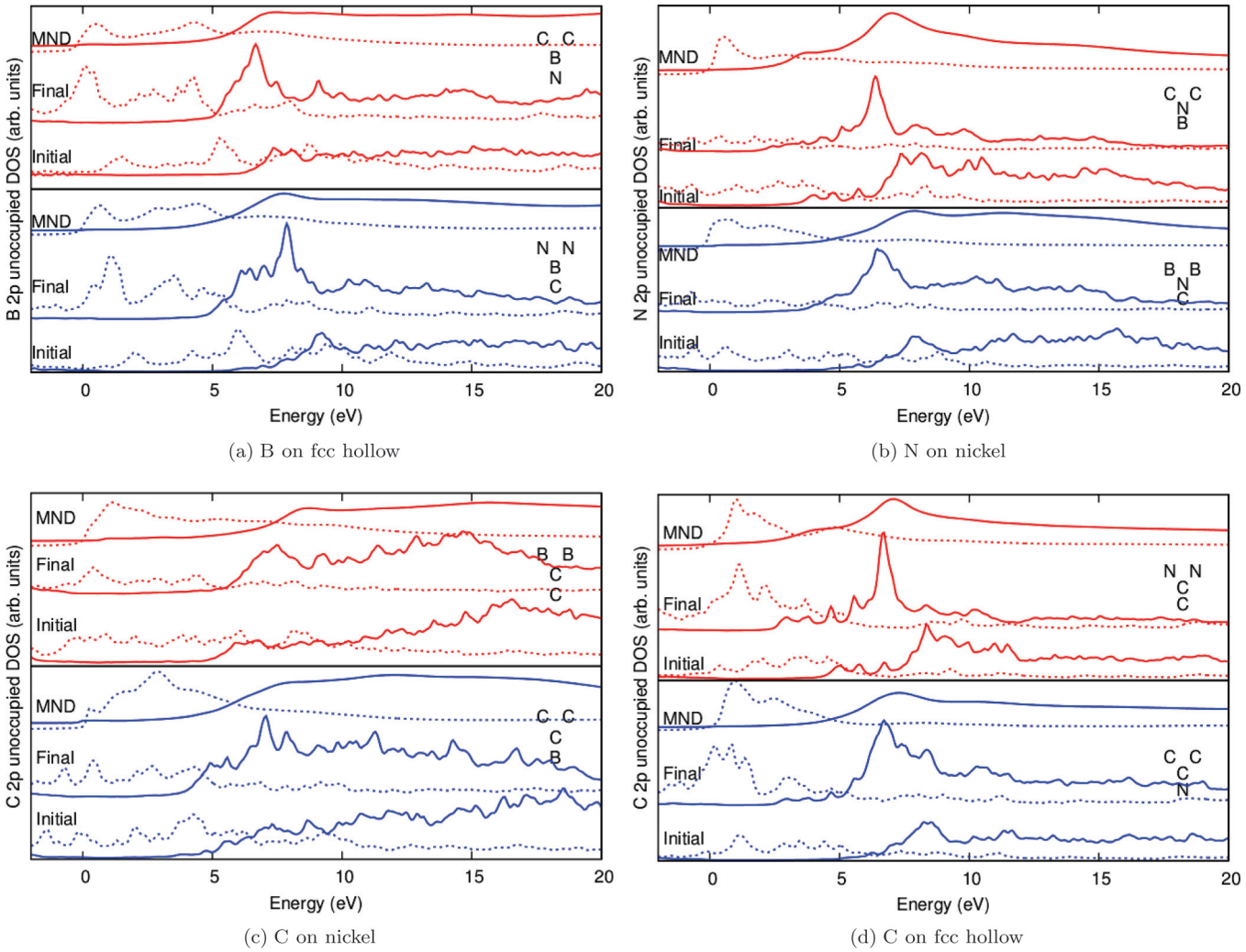

(a) B on fcc hollow (b) N on nickel

(c) C on nickel (d) C on fcc hollow

FIG. 4. (Color online) Initial-state (no core hole) and final-state (with 1s core hole) density of states and XAS calculated using MND theory, shown for all the constituent atoms of BC_2N^I (in the lower panels) and BC_2N^{II} (in the upper panels).

core-hole calculations by removing an electron from a selected core level—instead of using the $Z + 1$ approximation. We have used an atomic sphere radius of 1.35 a.u. for B, C, and N atoms. For the final-state calculations, we have constructed a supercell of size $2 \times 2 \times 1$, consisting of 40 atoms. The supercell size is large enough, owing to the metallic nature of the system and the screening that ensures the localization of the core-hole effect near the excited atom. This is corroborated by negligible (smaller than 0.02) charge fluctuations (compared to the initial state) on the neighbors of the excited atoms. The solution of the MND equation follows the implementation used in Ref. 30, including the normalization of the local density matrix. The energy range of the Green's function matrices was from -2 Ry up to 3 Ry (relative to the Fermi level set as zero), with a step of 0.005 Ry and smearing of 0.01 Ry.

Calculated spectra for C are depicted in Fig. 2. The solid (dotted) line represents the $\sigma^\star$ ($\pi^\star$) contributions to the XAS spectra. Computed spectra of C in graphene for both C on top of the fcc hollow site [Figs. 2(a) and 2(c)] and C on top of the nickel [Figs. 2(b) and 2(d)] coincide with the theoretical results of Ref. 30, where a very good agreement between theory and experiment was reported. As discussed previously, due to the preferential position of B (on the fcc hollow site) and N (on top of Ni) in BC_2N, the C atoms also have favorable locations, mentioned in the figure caption. The shape of the $\pi^\star$ peak clearly depends on the position of the C atom, because the π electron of the C atom bonds differently with the substrate depending on its position. For example, the p_z orbitals of the C atoms on top of the Ni atom and fcc hollow site overlap with the Ni $3d$ e_g and t_{2g} orbitals, respectively. This gives rise to the difference in the XAS (see Fig. 2); while the C on top of the Ni has one sharp $\pi^\star$ peak, two such peaks appear for the C on top of the fcc hollow site. Comparing with pristine graphene, we conclude that the presence of the B neighbors broadens and reduces the intensity of both the $\pi^\star$ and $\sigma^\star$ peaks of the C 1s spectra. On the other hand, N neighbors do not broaden the C 1s peaks.

Calculated spectra for B 1s and N 1s are illustrated in Figs. 3(a) and 3(b) and 3(c) and 3(d), respectively. Computed XAS for the B 1s (N 1s) in h-BN on the Ni, shown in Figs. 3(a) and 3(b) [Figs. 3(c) and 3(d)], are consistent with previous theoretical works [compare Figs. 3(a) and 3(d) with Fig. 3 in

Ref. 30). Similarly to the C, the shape of the $\pi^\star$ peak of the B and N 1*s* spectra also depends on how the π electron of the atom bonds with the substrate, determined by its position—on top of the nickel or fcc hollow site. Comparing with the pristine *h*-BN, we find that both the $\sigma^\star$ and $\pi^\star$ peaks of B 1*s* spectra become broadened in the presence of the C neighbors [see Fig. 3(a)]. However, the N $\pi^\star$ peak is the same in intensity and the $\sigma^\star$ spectra becomes sharper and stronger [see Fig. 3(d)] in BC_2N.

Dynamical core-hole screening is known to play an important role in x-ray absorption spectra of various carbon-based materials, such as graphite, C_{60}, carbon nanotubes, and graphene.[29,30,35] In order to investigate the extent of the core-hole screening effect in BC_2N (only energetically favorable unit cells have been considered here), we have plotted the initial and final state DOSs, along with the theoretically calculated XAS in Fig. 4. Since only the π states have finite DOSs at the Fermi level, they are responsible for the dynamical screening of the core hole. As B has fewer valence (π) electrons [note the gap in the initial state projected DOS of B in Fig. 4(a)], the 1*s* core hole is poorly screened. Due to this, a large peak appears just above the Fermi level in the final-state DOS. One can identify the origin of this sharp peak 2–3 eV above the Fermi level in the initial-state DOS [see Fig. 4(a)]. Note that, due to the poor screening, the MND calculation gives results very similar to the final-state DOS.

In contrast to B, the MND calculation result does not resemble the final-state DOS [see Fig. 4(b)] for N. This shows the importance of the electronic relaxation process in XAS. Since N has a sufficient number of valence (π) electrons [note the finite DOS in the initial state, shown in Fig. 4(b)], they screen the 1*s* core hole efficiently. The effective screening is so good that there is no sharp peak near the Fermi level in the final-state DOS, which is more or less shifted ∼1–2 eV downwards (compared to the initial-state DOS) due to the presence of the core hole. The case of C on nickel [see Fig. 4(c)] is similar to that of N, because of the sufficient core-hole screening. On the other hand, the case of C on the fcc hollow site [see Fig. 4(d)] is more like B, because of the low C DOS at the Fermi energy in the initial state. The nature of the screening can be intuitively understood from the electronegativity of the constituents: B < C < N. As N has the highest electronegativity, it attracts electrons from the neighboring B or C. This explains the lack of valence electrons for screening in the case of B or C on the fcc hollow site, both of which have N neighbors.

Until now, we have discussed either pure graphene/*h*-BN, or alloys. However, honeycomb B-C-N systems are also known to exist in phase-separated graphene and *h*-BN domains.[12] If the phase separation results in very large domains, the spectra are expected to look very similar to those of the parent phases. The spectral shape can change considerably, if smaller domains are present, because the interface region contributes significantly, in addition to the parent phases. Note that the atomic structure in the interface region has C-N and C-B bonds, which resemble local atomic arrangements in BC_2N. Hence, we can qualitatively predict the spectral shape of a graphene–*h*-BN mixture, by adding proper weights to the contributions from the parent phases and BC_2N. For example,

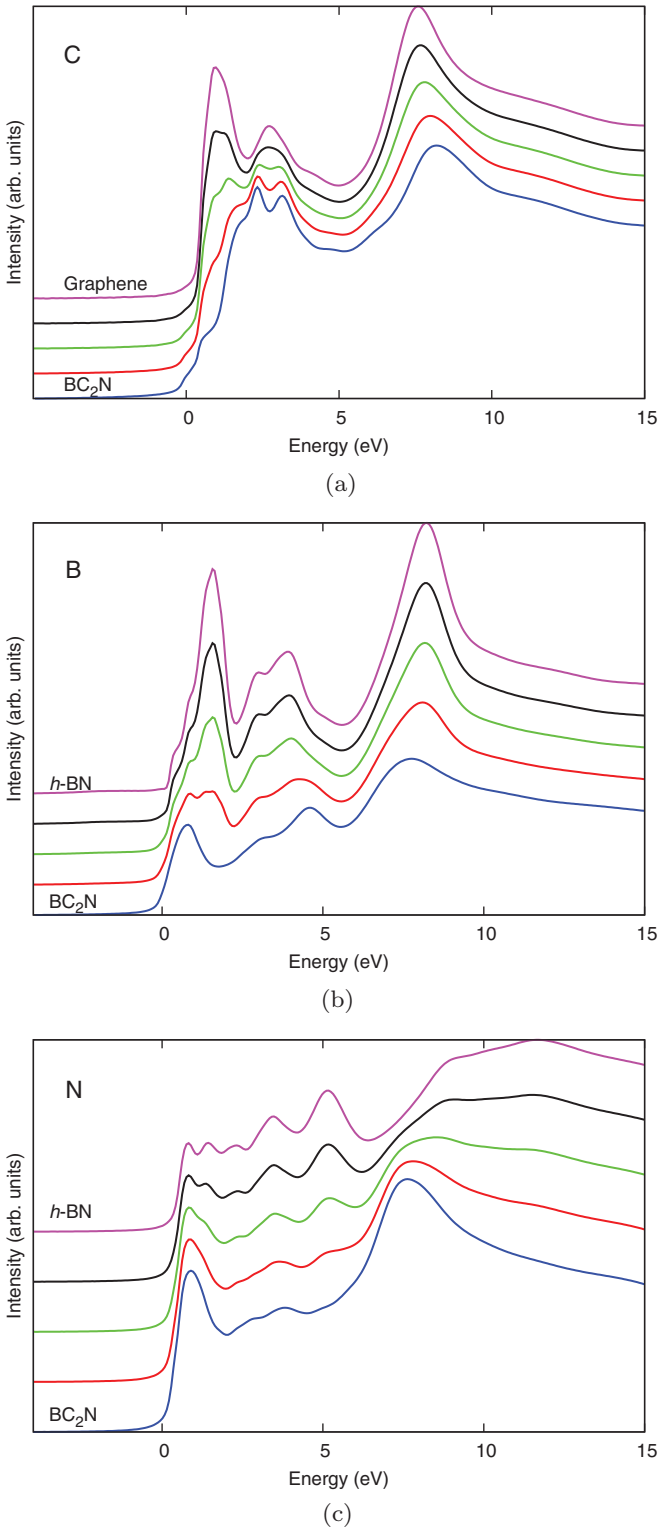

FIG. 5. (Color online) (a) C, (b) B, and (c) N *K*-edge spectra in graphene and *h*-BN phase-separated samples. In addition to the pure graphene and *h*-BN, the rest of the plots are for a mixture of 50% C and 50% BN. The top and bottom lines represent the pure phase and BC_2N spectra, respectively. In between these two extremes, the change in spectral shape (in the case of phase separation of graphene and *h*-BN) is illustrated as a function of increasing domain size (from bottom to top).

the C *K*-edge spectra in graphene has 100% contribution from graphene and 0% from BC_2N. On the other extreme, it has 0% contribution from graphene and 100% from BC_2N (taken as the average of BC_2N^I and BC_2N^{II}). The C *K*-edge spectrum of phase-separated grephene–*h*-BN mixture lies in between these two extremes and has contributions from the parent phase, as well as BC_2N. We illustrate the expected C, B, and N *K*-edge spectra, in graphene–*h*-BN samples of various degrees of phase separation in Figs. 5(a), 5(b), and 5(c), respectively.

In conclusion, we have computed, within the framework of MND theory, the B, C, and N *K*-edge XAS, where the constituent atoms are arranged in a honeycomb lattice. The MND calculation successfully reproduced the experimental XA spectra of graphene and *h*-BN,[30] and thus we expect it to work equally well for the mixed phases. In view of the recent enthusiasm for $B_xC_yN_z$ systems, our work can be useful for characterization of such materials. This can be further facilitated by recent developments in selective single-atom spectroscopy techniques.[36] Our work also reiterates the importance of dynamical core-hole screening in XAS, specifically for atoms like N and C on Ni, both having high density of the $2p$ states near the Fermi level. On the other hand, when there are fewer valence electrons available for the screening of the core hole, as in the case of B or C close to two N atoms with a high electronegativity, the MND calculations give very similar results to those of the final-state electronic DOS.

O.E. acknowledges support from VR, the KAW Foundation, and the ERC (Project No. 247062-ASD). J.R. acknowledges support from the Swedish Research Council and the Göran Gustafsson Foundation.

*somnath.bhowmick@uppsala.fysik.uu.se
†jan.rusz@uppsala.fysik.uu.se
‡olle.eriksson@uppsala.fysik.uu.se

[1] K. S. Novoselov, A. K. Geim, S. V. Morozov, D. Jiang, Y. Zhang, S. V. Dubonos, I. V. Grigorieva, and A. A. Firsov, Science **306**, 666 (2004).
[2] K. S. Novoselov, A. K. Geim, S. V. Morozov, D. Jiang, M. I. Katsnelson, I. V. Grigorieva, S. V. Dubonos, and A. A. Firsov, Nature (London) **438**, 197 (2005).
[3] A. H. Castro Neto, F. Guinea, N. M. R. Peres, K. S. Novoselov, and A. K. Geim, Rev. Mod. Phys. **81**, 109 (2009).
[4] K. S. Novoselov, D. Jiang, F. Schedin, T. J. Booth, V. V. Khotkevich, S. V. Morozov, and A. K. Geim, Proc. Natl. Acad. Sci. USA **102**, 10451 (2005).
[5] D. Pacilé, J. C. Meyer, Ç. Ö. Girit, and A. Zettl, Appl. Phys. Lett. **92**, 133107 (2008).
[6] J. C. Meyer, A. Chuvilin, G. Algara-Siller, J. Biskupek, and U. Kaiser, Nano Lett. **9**, 2683 (2009).
[7] C. Jin, F. Lin, K. Suenaga, and S. Iijima, Phys. Rev. Lett. **102**, 195505 (2009).
[8] A. Reina, X. Jia, J. Ho, D. Nezich, H. Son, V. Bulovic, M. S. Dresselhaus, and J. Kong, Nano Lett. **9**, 30 (2009).
[9] L. Huang, Q. Chang, G. Guo, Y. Liu, Y. Xie, T. Wang, B. Ling, and H. Yang, Carbon **50**, 551 (2012).
[10] C. Mattevi, H. Kim, and M. Chhowalla, J. Mater. Chem. **21**, 3324 (2011).
[11] L. Gao, J. R. Guest, and N. P. Guisinger, Nano Lett. **10**, 3512 (2010).
[12] L. Ci, L. Song, C. Jin, D. Jariwala, D. Wu, Y. Li, A. Srivastava, Z. F. Wang, K. Storr, L. Balicas, F. Liu, and P. M. Ajayan, Nat. Mater. **9**, 430 (2010).
[13] W. Zhao, S. M. Kozlov, O. Hofert, K. Gotterbarm, M. P. A. Lorenz, F. Vines, C. Papp, A. Gorling, and H.-P. Steinruck, J. Phys. Chem. Lett. **2**, 759 (2011).
[14] M. O. Watanabe, S. Itoh, K. Mizushima, and T. Sasaki, Appl. Phys. Lett. **68**, 2962 (1996).
[15] K.-T. Lam, Y. Lu, Y. P. Feng, and G. Liang, Appl. Phys. Lett. **98**, 022101 (2011).
[16] A. Y. Liu, R. M. Wentzcovitch, and M. L. Cohen, Phys. Rev. B **39**, 1760 (1989).
[17] P. Lu, Z. Zhang, and W. Guo, Appl. Phys. Lett. **96**, 133103 (2010).
[18] F. W. Averill, J. R. Morris, and V. R. Cooper, Phys. Rev. B **80**, 195411 (2009).
[19] J. Rossato, R. J. Baierle, T. M. Schmidt, and A. Fazzio, Phys. Rev. B **77**, 035129 (2008).
[20] J. Liang, S. Tang, and Z. Cao, J. Phys. Chem. C **115**, 18802 (2011).
[21] D. Pacilé, M. Papagno, A. Fraile Rodríguez, M. Grioni, L. Papagno, Ç. Ö. Girit, J. C. Meyer, G. E. Begtrup, and A. Zettl, Phys. Rev. Lett. **101**, 066806 (2008).
[22] W. Hua, B. Gao, S. Li, H. Ågren, and Y. Luo, Phys. Rev. B **82**, 155433 (2010).
[23] G. D. Mahan, *Many-Particle Physics* (Plenum, New York, 1990).
[24] P. Nozières and C. T. de Dominicis, Phys. Rev. **178**, 1097 (1969).
[25] T. Privalov, F. Gel'mukhanov, and H. Ågren, Phys. Rev. B **64**, 165115 (2001).
[26] T. Privalov, F. Gel'mukhanov, and H. Ågren, Phys. Rev. B **64**, 165116 (2001).
[27] R. Laskowski, T. Gallauner, P. Blaha, and K. Schwarz, J. Phys.: Condens. Matter **21**, 104210 (2009).
[28] O. Wessely, M. I. Katsnelson, and O. Eriksson, Phys. Rev. Lett. **94**, 167401 (2005).
[29] O. Wessely, O. Eriksson, and M. I. Katsnelson, Phys. Rev. B **73**, 075402 (2006).
[30] J. Rusz, A. B. Preobrajenski, M. L. Ng, N. A. Vinogradov, N. Mårtensson, O. Wessely, B. Sanyal, and O. Eriksson, Phys. Rev. B **81**, 073402 (2010).
[31] V. I. Grebennikov, Y. A. Babanov, and O. B. Sokolov, Phys. Status Solidi B **79**, 423 (1977).
[32] We did not take the fully relaxed structures of BC and NC (sp^3 in nature) for spectral calculations. Since we focus on B-C-N alloys forming a two-dimensional honeycomb lattice, we considered the sp^2-bonded, planar structure of BC and NC, similar to the monolayer *h*-BN.
[33] P. Giannozzi, S. Baroni, N. Bonini, M. Calandra, R. Car, C. Cavazzoni, D. Ceresoli, G. L. Chiarotti, M. Cococcioni, I. Dabo, A. Dal Corso, S. de Gironcoli, S. Fabris, G. Fratesi, R. Gebauer, U. Gerstmann, C. Gougoussis, A. Kokalj, M. Lazzeri, L. Martin-Samos, N. Marzari, F. Mauri, R. Mazzarello, S. Paolini, A. Pasquarello, L. Paulatto, C. Sbraccia, S. Scandolo, G. Sclauzero,

A. P. Seitsonen, A. Smogunov, P. Umari, and R. M. Wentzcovitch, J. Phys.: Condens. Matter **21**, 395502 (2009).

[34]P. Blaha, K. Schwarz, G. K. H. Madsen, D. Kvasnicka, and J. Luitz, computer code WIEN2K (Technische Universität Wien, Austria, 2001).

[35]O. Wessely, M. I. Katsnelson, A. Nilsson, A. Nikitin, H. Ogasawara, M. Odelius, B. Sanyal, and O. Eriksson, Phys. Rev. B **76**, 161402 (2007).

[36]O. L. Krivanek, M. F. Chisholm, M. F. Murfitt, and N. Dellby, Ultramicroscopy **123**, 90 (2012).